REPORT DOCUMENTATION PAGE

AFRL-SR-AR-TR-02-

0420

1. AGENCY USE ONLY *(Leave blank)*	2. REPORT DATE	3. REPORT TYPE AND DATES COVERED
		01 APR 98 TO 31 DEC 01 FINAL

4. TITLE AND SUBTITLE
ASSERT98 ULTRAFAST GASA PHOTOCONDUCTIVITY AND APPLICATIONS FOR RADIATION-HARD ELECTRONICS

5. FUNDING NUMBERS
61103D
3484/TS

6. AUTHOR(S)
DR WHITAKER

7. PERFORMING ORGANIZATION NAME(S) AND ADDRESS(ES)
UNIVERSITY OF MICHIGAN
1058 WOLVERINE TOWE-DRDA
3003 S. STATE STREET
ANN ARBOR MI 48109-1274

8. PERFORMING ORGANIZATION REPORT NUMBER

9. SPONSORING/MONITORING AGENCY NAME(S) AND ADDRESS(ES)
Department of the Air Force
Air Force Office of Scentific Research
801 N. Randolph St Rm 732
Arlington. VA 22203-1977

10. SPONSORING/MONITORING AGENCY REPORT NUMBER

F49620-98-1-0365

11. SUPPLEMENTARY NOTES

12a. DISTRIBUTION AVAILABILITY STATEMENT
Distribution Statement A. Approved for public release; distribution is unlimited.

12b. DISTRIBUTION CODE

13. ABSTRACT *(Maximum 200 words)*
Finally, in the last year of the AASERT and during a no-cost extension period, an effort was made to demonstrate how pulsed, single-cycle terahertz beams generated and detected by nonstoichiometric-GaAs dipole antennas - could be employed as a tool for the imaging of metal and dielectric objects. This was accomplished through the use of the time-reversal and back-propagation of time-domain signals scattered from objects through off-axis diffraction. Experimental methods were devised and applied to the reconstruction of onc- and two-dimensional objects in both transmissive and reflective geometries. The images produced in both simulation and experiment were able to resolve features less than both the peak and mcan wavelengths of the broadband THz pulses. It was empirically illustrated that this technique should be able to produce images rivaling those of an ideal diffraction-limited imaging system. Images comparable to those produced by conventional, direct (non-scattering) 1Hz imaging systems were also produced. These results from the time-domain, THz, off-axis imaging have a great deal of potential and hold promise that objects can be identified not just by their scattered time-domain signatures, but actually by their reconstructed shapes.

20030106 099

14. SUBJECT TERMS	15. NUMBER OF PAGES
	16. PRICE CODE

17. SECURITY CLASSIFICATION OF REPORT	18. SECURITY CLASSIFICATION OF THIS PAGE	19. SECURITY CLASSIFICATION OF ABSTRACT	20. LIMITATION OF ABSTRACT
Unclassified	Unclassified	Unclassified	UL

AASERT 98: Ultrafast GaAs Photoconductivity and Applications for Radiation-Hard Electronics

Final Report

Grant No. F49620-98-1-0365

For the Period 1 April, 1998 - 31 December, 2001

DISTRIBUTION STATEMENT A
Approved for Public Release
Distribution Unlimited

Principal Investigator
Dr. John F. Whitaker

University of Michigan
Ultrafast Science Laboratory
2200 Bonisteel Blvd., Room 1006
Ann Arbor, MI 48109-2099

Executive Summary

I. Significant Advancements and Conclusions

The primary goal of this AASERT augmentation award has been to introduce a new and potentially revolutionary methodology into the investigation of the radiation tolerance of high-frequency digital circuits, especially in terms of circuit malfunctions resulting from single-event effects. Specifically, the application of an ultrafast-response, high-impedance, nonstoichiometric-GaAs probe and sampling gate to the measurement of waveforms at internal nodes of a digital circuit has revealed that one can observe an accurate, nearly real-time view of the way in which individual IC components respond as the circuit conditions change. In particular, when an ultrashort laser pulse emulating a high energy cosmic particle irradiates and injects charge at a given location within a circuit, the nonstoichiometric GaAs photoconductive probe (PC probe) can monitor the circuit's reaction, as well as the impact on the repetitive clock signal, at a wide variety of positions. As a result, this type of characterization tool has been demonstrated for the first time, with a high-speed InP digital circuit utilizing heterojunction bipolar transistors in an ECL-like technology. Perhaps most interesting was the direct observation that for sufficiently energetic laser-excitation pulses, and during operation at especially high clock frequencies, the photogenerated charge within the bipolar transistor would maintain the transistor in an "on state" for numerous cycles. Despite the fast relaxation characteristics exhibited by InP, the presence of the injected charge would cause a loss of information for a duration of as many as five cycles (with a clock of 10 GHz), even though designers often assume that only a single clock cycle would be affected. Overall, the results of this part of the program were significant because they showed that there can be direct information provided to circuit designers about how susceptible their circuit is to losing a bit (or bits) of data as a function of where within the circuit a charge pulse is injected and when within the clock cycle the upsetting laser or radiation pulse strikes.

In addition to the application of the nonstoichiometric-GaAs PC probe for specialized digital circuit testing, we have demonstrated that it is possible to expand its role to the testing of nonlinear microwave circuits through inspection of internal-node periodic waveforms in the time domain. We have thus investigated for the first time the operation of class E and F microwave amplifiers (in which the circuit transistor behaves as a switch) – as well as frequency multipliers – from within the interior of the circuit. The use of the high-impedance, high-speed probe was crucial here, as the class of operation of the amplifier is only verifiable when one can observe the shape of the switch waveforms. In fact, this study demonstrated that Class E and F amplifiers with record-breaking efficiencies at 8 GHz were truly operating in the correct mode. In the absence of good large-signal models for the power transistors utilized in the circuits, the nonstoichiometric-GaAs PC-sampling probe was able to substantiate the approximate design method that was based on small-signal device parameters. Thus, successful measurements were able to remove any ambiguity about the specific class of operation of the circuit and definitively validate the microwave circuit design. Furthermore, the measurements on the multiplier circuits

2

were able to extract all the harmonic content on both the input and output networks, pinpointing, for instance, where additional harmonic tuning was required.

Finally, in the last year of the AASERT and during a no-cost extension period, an effort was made to demonstrate how pulsed, single-cycle terahertz beams – generated and detected by nonstoichiometric-GaAs dipole antennas – could be employed as a tool for the imaging of metal and dielectric objects. This was accomplished through the use of the time-reversal and back-propagation of time-domain signals scattered from objects through off-axis diffraction. Experimental methods were devised and applied to the reconstruction of one- and two-dimensional objects in both transmissive and reflective geometries. The images produced in both simulation and experiment were able to resolve features less than both the peak and mean wavelengths of the broadband THz pulses. It was empirically illustrated that this technique should be able to produce images rivaling those of an ideal diffraction-limited imaging system. Images comparable to those produced by conventional, direct (non-scattering) THz imaging systems were also produced. These results from the time-domain, THz, off-axis imaging have a great deal of potential and hold promise that objects can be identified not just by their scattered time-domain signatures, but actually by their reconstructed shapes.

II. Personnel Involved in the Research Effort

(a) Augmentation Award students directly supported

Mathew Crites	17 months
Jonathan Berry	8 months
A. B. Ruffin	5 months
Eric Pooler	6 months

(both Crites and Berry left graduate school early without completing their PhD; Ruffin graduated during the AASERT program)

(b) Associated personnel

Dr. John Whitaker	PI & advisor
Prof. Ted Norris	Consultations
Joan Decker (visiting research fellow)	computer algorithms
Dr. Gerhard David	Post-doctoral fellow/Mentor
Kyoung Yang	Graduate student/Mentor
J. Van Rudd (Picometrix)	Working under an AFOSR SBIR, Picometrix provided helpful advice and equipment to

the project.

III. Publications Resulting from the Research Effort

(1) T.R. Weatherford, J. Whitaker, K. Jobe, S. Meyer, M. Bustamante, S. Thomas III, and K. Elliott, "Analysis of single-event-induced voltage transients in InP-based HBT circuits," *Journal of Radiation Effects* Vol. 19-1 (July 2001).

(2) A. B. Ruffin, J. Decker, L. Sanchez-Palencia, L. Le Hors, J. F. Whitaker, and T. B. Norris, "Time Reversal and Object Reconstruction Using Single-Cycle Pulses," *Optics Lett.,* vol. 26, pp.681-683 (May 2001).

(3) M. Weiss, M. Crites, E. Bryerton, J. Whitaker, and Z. Popovic, "Time-domain optical sampling of switched-mode microwave amplifiers and multipliers," IEEE *Trans. Microwave Theory Tech.,* vol. 47, pp. 2599-2604 (Dec. 1999).

(4) J.F. Whitaker, G. David, and M. Crites, "Integrated-circuit diagnostics using micromachined photoconductive-sampling probes," OSA *Trends in Optics and Photonics*, J.E. Bowers and W.H. Knox, eds., (Optical Society of America, Washington, DC 1999), pp. 158-161.

(5) G. David, T. Yun, M. Crites, J.F. Whitaker, T.R. Weatherford, K. Jobe, S. Meyer, M. Bustamante, W. Goyette, S. Thomas III, and K. Elliott, "Absolute potential measurements inside microwave digital ICs using a micromachined photoconductive sampling probe," IEEE *Trans. Microwave Theory Tech.,* vol. 46, pp. 2330-2337 (Dec. 1998).

(6) G. David, K. Yang, M. Crites, J.-S. Rieh, P. Bhattacharya, L.P.B. Katehi, and J.F. Whitaker, "Photoconductive probing and computer simulation of microwave potentials inside a SiGe MMIC," in IEEE Topical Meeting on Silicon Monolithic Integrated Circuits in RF Systems, S. Kayali, Ed. (IEEE, Piscataway, NJ, Sept. 1998), pp. 187-191.

IV. Invited Conference Presentations

(1) A.B. Ruffin, J. Whitaker, T. Norris, J. Decker, L. Sanchez-Palencia, L. LeHors, and J.V. Rudd, "Time reversal and object reconstruction using single-cycle terahertz pulses," presented at the 2000 IEEE Lasers and Electro-Optics annual meeting, Puerto Rico, Nov. 2000.

(2) J.F. Whitaker "Advances in Optically-Based Sampling for Diagnostics of Microwave Digital and Analog Circuits," presented at the Conference on Lasers and Electro-Optics – Pacific Rim, Sept. 1999.

(3) J.F. Whitaker, G. David, and M. Crites, "Integrated-circuit diagnostics using micromachined photoconductive-sampling probes," presented at the OSA Topical Conference on Ultrafast Electronics and Optoelectronics, April 1999.

Detailed Technical Accomplishments

As mentioned in the executive summary, the accomplishments under this AASERT program have contributed to the success of several research areas. That a relatively small grant was able to significantly contribute to multiple areas was due to the fact that students left graduate school unexpectedly on two occasions in the middle of this AASERT, and so on short notice new students who had already started their thesis research in somewhat different areas were supported. Fortunately, these different areas were all tied together by their use of nonstoichiometric, low-temperature-grown GaAs as a fast photoconductive sampling gate. This section provides technical details about the results from each of these research areas.

(1) *Radiation-tolerance testing of microwave digital circuits*

In this AASERT, we investigated for the first time the operation of a microwave digital circuit from the interior of the network in order to evaluate the tolerance of the circuit to radiation effects, which have been simulated by the optical injection of charge. A nonstoichiometric-GaAs photoconductive (PC) probe, described in detail in the reports of the original parent grant of this AASERT, was used as an internal-node, high impedance, on-wafer probe in order to learn in which specific locations and for how long internal circuit operation was disrupted by the optically-injected charge. As a result of this study, we have shown that it is possible to employ a high-bandwidth, high-impedance probe to gain valuable information that will help determine what characteristics of a circuit are responsible for it being susceptible to optical charge injection over an unacceptably long period of time.

This work has been carried out on a high-speed inverter, consisting of two D-flip-flops and incorporating heterojunction bipolar transistors (HBT) in InP technology. Indium phosphide has been used in this case rather than GaAs because Hughes Electronics was readily willing to make this circuit available for us to work with. Two different types of characterization experiments were devised using the nonstoichiometric-GaAs probes, one involving exclusively the measurement of photoexcited transients, and the other capturing the internal clock waveforms as the same photoinjected charge transients are produced. It was necessary to prove that an effective procedure could be established for the former technique before the second technique for actual radiation-tolerance testing could be developed.

The experiment to observe the response of a single transistor to a laser-pulse stimulus (in order to emulate the irradiation of the device by a cosmic particle) can be described as follows. The digital circuit is connected within a test fixture so that a dc bias for its active devices and an electrical ground are provided. Since the goal here is not to test the circuit under clocked operation, but to observe the upset response duration from a single device, the circuit input is also tied to a dc bias. In this way one can set up the first transistor in the circuit so that it is either "on" and drawing current or "off" and not drawing current. As we discovered, if short laser pulses were delivered to this transistor when it was biased "off," then charge was injected so that the transistor was turned "on," and a transient at the collector could be resolved using the PC probe. The interconnects within this circuit were 3-μm wide and not densely packed, and thus our 7-μm-wide probe tip was easily able to make a high-impedance connection at virtually every

node. There was also no passivation on the signal lines of this circuit (some current supply lines were passivated), and thus the absolute voltage values of the transients and the dc levels could be obtained using our PC probe. While we were also able to measure the transient signal switched from the illuminated HBT as it propagated to subsequent devices and affected a change in their outputs, we will concentrate here on the signal at the collector of the first HBT. The duration of this signal is of fundamental significance, as the time during which the circuit is affected by the laser-injected charge can be deduced most easily by decreasing the HBT response time (and thus increasing the tolerance to radiation at the generation site).

The experiment was conducted in the standard, "pump-probe" configuration, with excitation and sampling accomplished using the same 100-fs-duration laser pulses from a Ti:sapphire oscillator. That is, each pulse is divided using a beam splitter, and one beam is variably delayed with respect to the other (see Fig. 1). The excitation beam was focused down to a diameter of several micrometers and was guided to a point directly over the first HBT in the microwave digital circuit using a single-mode optical fiber with a "bulb" focusing element formed on its tip during cleaving. The probe beam was coupled into a second optical fiber, which led to the photoconductive sampling gate on the PC probe. The output from the PC probe, buffered by a high-impedance source follower, was sensed by a lock-in amplifier that was synchronized to an RF synthesizer. This synthesizer drove the acousto-optic modulator that chopped the pump beam.
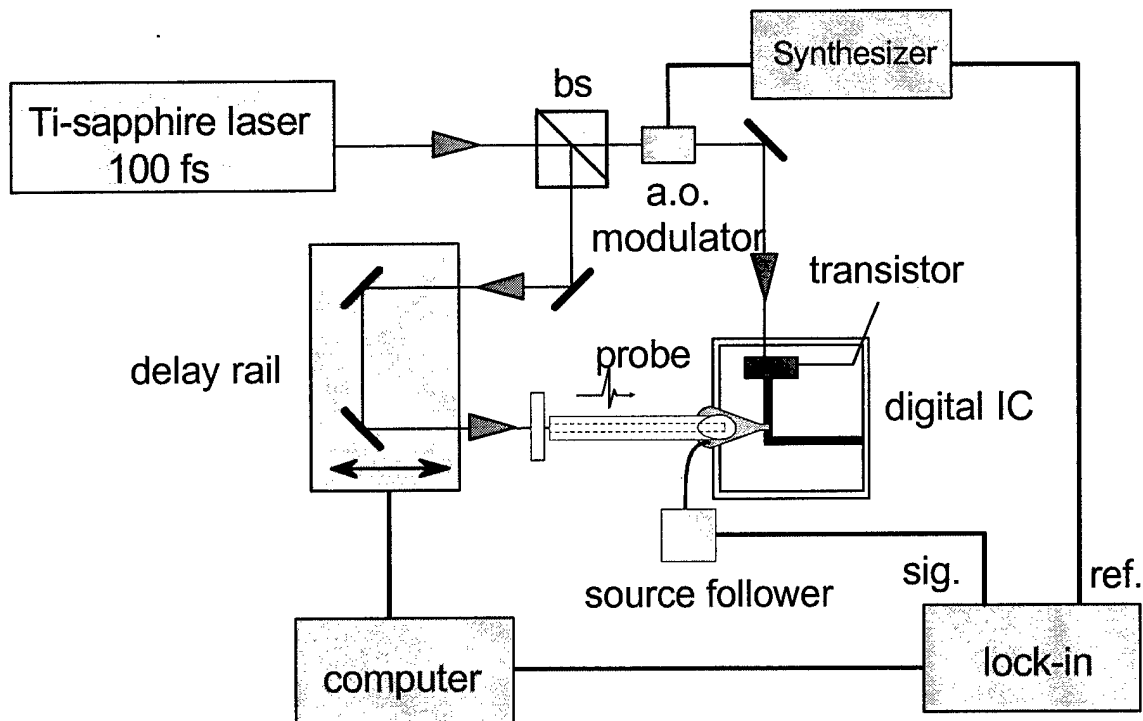

Figure 1. Schematic of the experimental set-up used to characterize the response of an HBT internal to a microwave digital circuit that was illuminated by a several-hundred-femtosecond-duration laser pulse. The charge thus injected is meant to emulate the transient charge expected when a cosmic particle would irradiate a device.

A close-up photograph of a device mounted in the PC probe test environment is shown in Fig. 2. (This device is a silicon-on-insulator [SOI] test circuit provided by AFRL.) The single-mode optical delivery fiber that carrier the probe-beam ultrashort optical pulse train enters from the upper left, where it is fixed to the triangular-shaped printed circuit board (that also holds the JFET source follower package). The fiber then reappears at the narrow end of the circuit board, extending for approximately half a centimeter to the point where the fiber is polished to a 45° angle and the PC probe is mounted. The microscope objective is used here instead of the "bulbed" fiber in order that the simulated radiation excitation beam can be focussed to a smaller spot size.

For the InP circuit measurements, the PC probe contacted the HBT that was to be illuminated at its output terminal, the collector, as mentioned above. When the delay was set so that the probe pulses preceded the pump pulses, then a base-line dc level was observed at the output of the PC probe. However, as the optical delay was scanned so that the probe pulses arrived after the pump pulses injected charge into the HBT, the output of the PC probe tracked the transient response of the HBT to the injected charge. A typical trace obtained from this HBT is shown in Fig. 3.
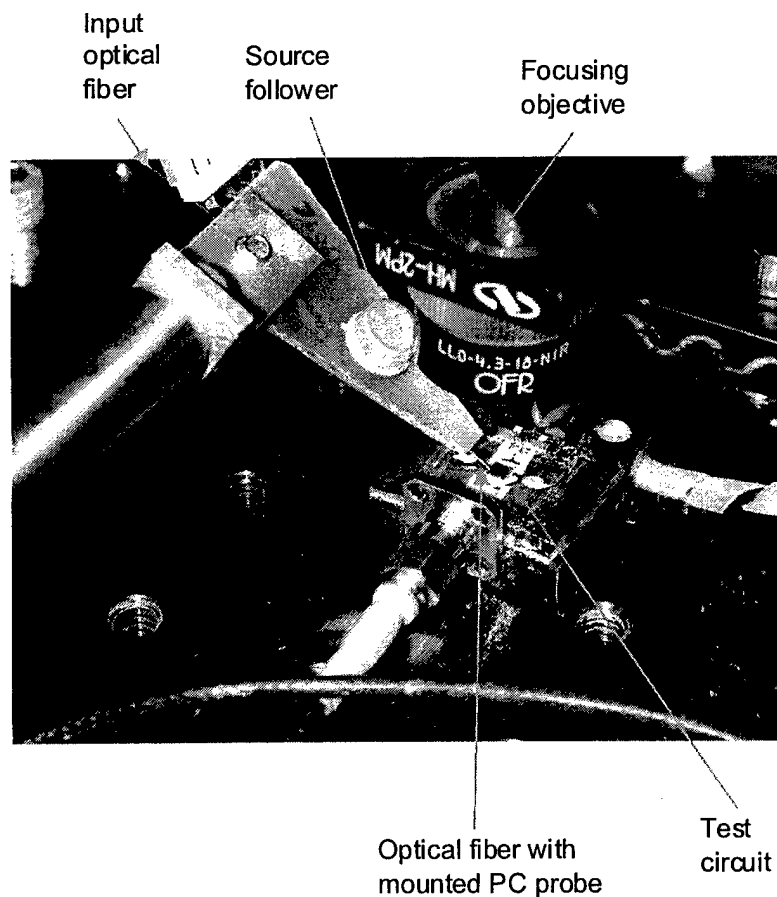

Figure 2. Detail of a photoconductive probe measurement of an SOI circuit from AFRL.
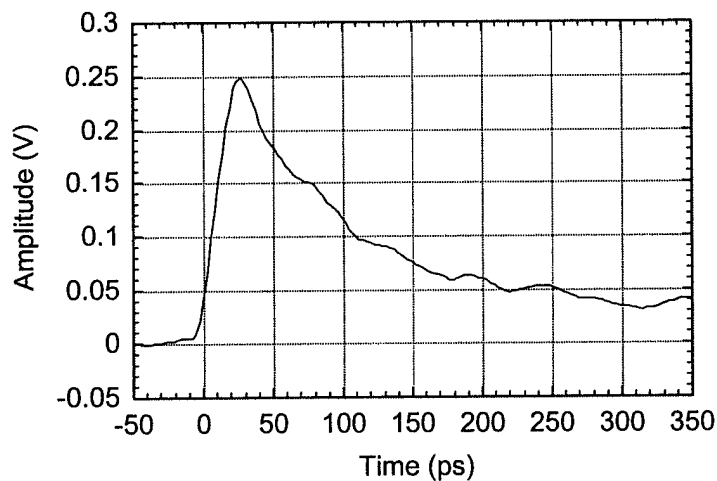
Figure 3. Transient output directly observed on the collector of an HBT illuminated by an ultrafast laser pulse.

The rise time of the HBT output transient is observed to be about 20 ps, which is more than four times greater than the time-response limit of the PC probe. Therefore, one may speculate that there is some capacitance associated with the device that needs to be charged before the peak of the signal is reached at the collector. The signal decays with a multiple exponential behavior, the first time constant being around 8 ps, and the second nearly 81 ps. A long tail stretching out in time past the delay duration that was attainable with the variable optical path length was also observed, although there is some evidence that the length of this tail may depend on the intensity of the laser illumination. One possible implication here is that if the circuit was clocked when the laser upset pulse, emulating the charge injection of a cosmic particle, illuminated the HBT, then depending on when the laser pulse arrived relative to the clock features, one or perhaps several cycles of the clock would be adversely affected as the HBT relaxed back to its undisturbed state. Thus, particularly for high-frequency operation, significant amounts of information could be lost.

In order to attempt to determine if the substrate relaxation dictates the response of the HBT, we have continued by characterizing the lifetime of photoexcited carriers in the same InP wafer used to fabricate the microwave digital circuit tested. The relaxation of the bulk InP also follows the form of a multiple exponential. The initial $1/e$ time is 6 ps, while the second exponential has a time constant of 160 ps. A small tail response with an extremely long relaxation time is also present. The initial, 6-ps time constant appears to last too long to be explained by carrier cooling within the InP conduction band. On the other hand, given the InP band gap (~1.35 eV), the 1.53-eV photon energy of the 810-nm-wavelength laser light used for the lifetime characterization does excite the carriers nearly 200 meV above the conduction band minimum, and perhaps there is sufficient scattering and cooling to extend the initial time constant to several picoseconds. It is apparent from these measurements that there are some circuit parasitics that control the HBT response measured by the PC probe.

With the accomplishment of *in situ* transient generation and measurement utilizing the fiber-mounted, nonstoichiometric GaAs probe, it was then possible to extend the technique one step further so that observations of the effects of laser-transient excitation on clock-waveform

8

degradation could be made. It was thus necessary to devise a new ultrafast measurement method that employed the pulse train from one mode-locked laser to emulate the single-event-inducing, high-energy-radiation impulse, while utilizing the pulse train from a second mode-locked laser, phase-locked to the circuit microwave input signal, as the sampling pulses. In this type of measurement, the mechanical variable delay that we could easily impose between the pump and probe beams (that have repetition rates that differ by approximately 1 KHz) was insufficient to capture the time duration of many cycles of a typical circuit clock waveform. Since it is necessary to observe the possibly long-lived effect of the charge injected by the optical upsetting pulse, one needs to consider a number of clock cycles after the point in time during which the charge was injected. This new technique employing multiple lasers operating at slightly different repetition frequencies insured that we would capture all of the distortion that could be created by the upset laser pulse.

The principal experimental setup for our measurement of laser-upset, high-frequency-clocked digital ICs is sketched in Fig. 4. It consists of two femtosecond laser systems, and the LT-GaAs micromachined photoconductive sampling probe, which has a temporal resolution of 3 ps. The first Ti:sapphire laser is used to irradiate a sensitive location within an active device inside the circuit. It has a phase-locked-loop feedback system that controls the laser cavity length, so that a highly stable 80-MHz laser repetition rate and synchronization with an external oscillator are achieved. Phase-locking of a microwave synthesizer (used as the circuit clock) with this laser oscillator is possible via a 10 MHz reference signal output from the laser phase-locked-loop control box. The microwave synthesizer delivering the circuit clock is thus phase-locked with the laser system exciting the single-event upset. The clock frequency is set exactly to a multiple of the laser repetition rate, and the time delay of the laser pulses with respect to the clock waveform is obtained using the built-in feedback electronics of the laser system. This allows one to determine whether circuit operation is susceptible to radiation-induced charge injection over the entire clock cycle, or just a certain part of the clock cycle.

Optical pulses from the second laser, which operates at a repetition frequency of 80 MHz plus an offset frequency in the order of 100 Hz, are used to gate the photoconductive probe so that an equivalent-time sampling scheme can be employed. The setup uses a phase referencing technique to synchronize the clock waveform and electrical upset transient with the gating laser in order to cancel out timing fluctuations. The reference signal is generated by an RF mixer, with the LO provided by the mixed-down output signal of two fast photodiodes that are illuminated each by one of the fs lasers. The IF signal triggers a digitizing oscilloscope that records the downconverted waveform of the sampled clock signal/electrical transient at the probed node, including the dc offset. This scheme provides a time window of 12.5 ns before the next laser pulse arrives, yielding adequate time to observe many cycles after the onset of the upset event.

Measurement examples using a digital InP heterojunction bipolar transistor (HBT) frequency divider circuit as the device under test demonstrated the unique capabilities of the photoconductive probe to interrogate the internal operation of a circuit under hypothetical radiation conditions. The circuit provided a differential divide by four output based on a differential input clock and was nominally designed to operate at 3.5 GHz. The divider has, however, been successfully operated at input frequencies up to 18 GHz.

Figure 4. Schematic of the new experimental set-up used for in situ *photoconductive sampling of high-frequency clock waveforms that are extracted to determine the susceptibility of a circuit to single-event effects.*

Figure 5 shows the in-circuit waveforms at the collector of the first HBT within a differential pair in an inverter section, while a laser pulse is incident on the same HBT. The clock input is set at a frequency of only 240 MHz in this instance. The lensed fiber is used to illuminate the transistor with the optical pulses over a focus diameter of ~ 5 micrometers. Three clock cycles can be observed in the figure, and the laser arrives during the center cycle visible in the time window. If the laser pulse strikes the HBT when the maximum voltage of the clock signal (off state) is present, an actual single-event upset (SEU) is detectable at the circuit output, and the measurement result reveals a highly disturbed waveform inside the circuit (Fig. 5 (a)). If the laser pulse arrives during the minimum potential (on state), an SEU is not observed at the circuit output, and the clock cycle is not strongly disturbed (Fig. 5 (b)). Figure 6 shows the SEU transient of Fig. 5 (a) in more detail. The transient has a rise time of about 8 ps and a length of 70 ps. These results reveal that the SEU susceptibility depends on the relative phase between the SEU transient and the clock signal, and, using the photoconductive sampling head, the period of the clock cycle during which the circuit is sensitive to the SEU can be precisely determined.

This point is illustrated more dramatically in Fig. 7 for distorted, 2.4-GHz-frequency clock waveforms measured after one of the HBTs further into the inverter was illuminated with the ultrafast laser pulses. For an arrival time of the excitation laser pulses that is at the onset or even the middle of the 'on-state,' corresponding to the curves marked t_1 or t_2 in the figure, respectively, there is very little effect on the successive 'high' voltage state. There is also no evidence at the output of the entire circuit of a single-event upset that disturbed the divide-by-four operation. However, when the laser upset pulse arrives during the rise time of the 'off-state,' then virtually the entire 'high' portion of the clock cycle is disrupted (curve t_3), and the

divide-by-four output of the circuit is temporarily interrupted. More of the clock cycle is lost than for the result of Fig. 5 because of the higher clock frequency in Fig. 7. It is thus expected that for higher and higher clock frequencies, numerous clock cycles could be obliterated, and many bits of data lost.
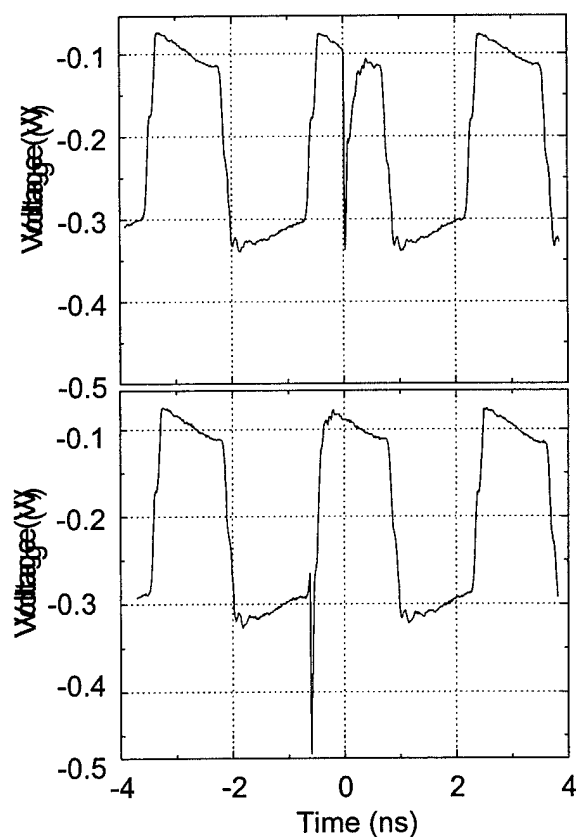

Figure 5. Electrical transient measured inside a digital circuit during (a) 'off-state' and (b) 'on-state' operation (240 MHz clock frequency).
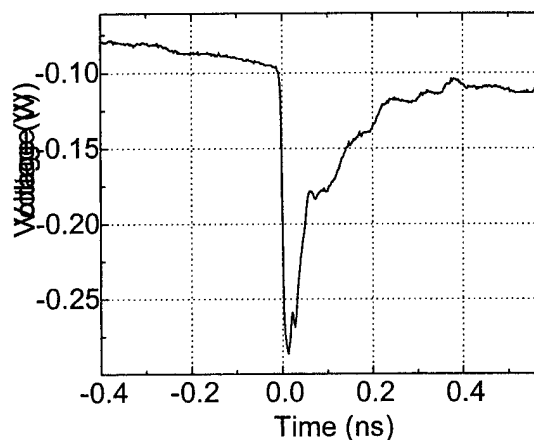

Figure 6. Photoexcited transient of Fig. 5(a) observed with higher time resolution.

11
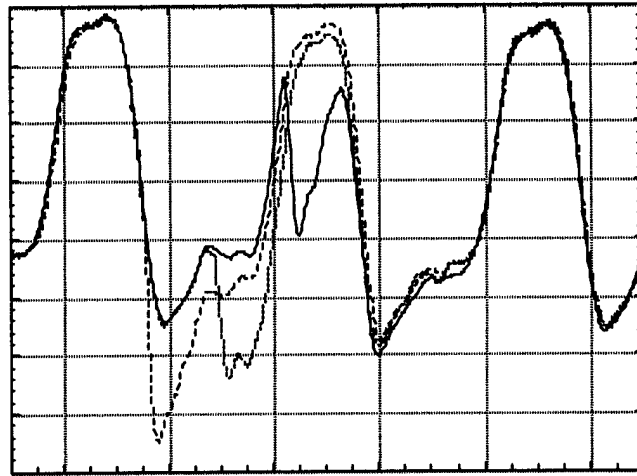
Figure 7. Clock-cycle distortion as a function of arrival of upsetting laser pulse (2.4 GHz clock frequency).

This is actually illustrated in Fig. 8 for the situation where the clock input is increased up to 10 GHz, with the PC probe capturing the circuit waveform at the same location as for Fig. 7. Here the potentially catastrophic elimination of five clock cycles – detrimental due to the fact that if transients exceed more than one clock period, the ability to detect and correct multiple bit errors in a bit stream becomes difficult – can be observed. This result more than any other demonstrates that the PC probing technique with the nonstoichiometric GaAs PC probe can be very useful for confirming how ultra high speed digital circuits will be vulnerable to single events.
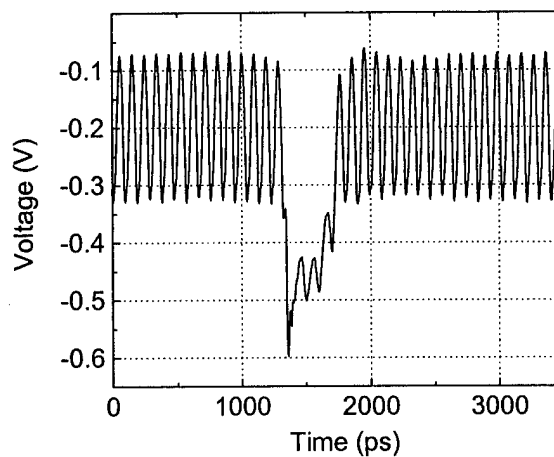
Figure 8. Clock-cycle distortion for a 10 GHz clock frequency.

12

(2) *Nonstoichiometric-GaAs PC probe applications to nonlinear microwave circuits*

The flexibility of the nonstoichiometric-GaAs probe in circuit diagnostics has also been demonstrated within the AASERT program through characterization of several nonlinear microwave circuits – an 8-GHz high-efficiency power amplifier and 1- and 5-GHz frequency doublers. In these nonlinear measurements, it is very valuable to determine the temporal nature of the waveforms at intermediate locations within the circuit, since only these waveforms can reveal the microwave harmonic behavior and whether its evolution is correct.

For instance, in order to analyze nonlinear amplifiers designed to deliver a sinusoidal wave to the load, voltages at characteristic points inside the circuit need to be known. If large-signal models of the transistor are available, the time-domain waveforms at the switch can be simulated using harmonic balance methods to demonstrate the offset between the current and voltage waveforms. If these models are not available, as is often the case (especially at higher frequencies), or if one would like to confirm the presence of harmonics and the effectiveness of filtering in certain circuit elements, then the photoconductive probe becomes an extremely valuable tool. In multipliers, for instance, waveform measurements are able to track harmonic leakage, which can be used to expedite the design cycle. In amplifiers, simply achieving high output power is one way to verify performance, but this leaves an ambiguity in the specific class of operation, and thus does not validate the design.

An example of the types of circuits tested is shown in Fig. 9, in which a class-F amplifier is depicted along with five test points. The active MESFET device is marked by the letters **FLK**, while the input circuit, on the left, performs a matching function and also acts as a filter to remove any reflected harmonics. The output circuit on the right also filters out harmonics and provides the correct load to the transistor at the fundamental frequency.
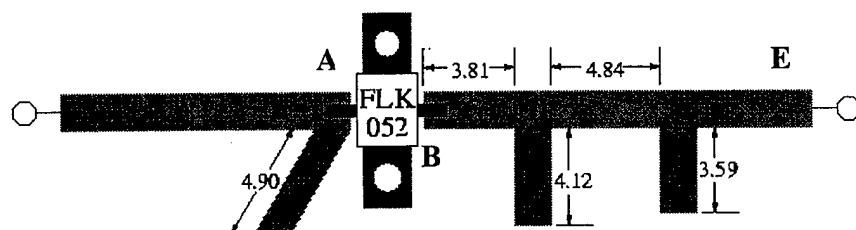

Figure 9. General outline of the tested high-efficiency circuits. Dimensions are in millimeters.

In Fig. 9, point **A** represents the input plane of the amplifier, where the input circuit should filter out any harmonics reflected to the gate from the drain of the transistor, and the waveform should be sinusoidal. As seen in Fig. 10 this waveform was found to be sinusoidal, and since there was very little harmonic behavior, we were able to conclude that there was no significant harmonic content reflected back to the amplifier input. The waveform at point **E** would also be a sine wave if proper filtering was taking place, and indeed in Fig. 10 we measured a sinusoid, and one with significantly higher amplitude than the input. The output circuit of the

13

amplifier then presumably achieved success in filtering out the harmonics of the switched waveforms that were discovered closer to the active device (and measured at points **B**, **C**, and **D**), and the circuit performed as an amplifier of the input waveform.

Point **B**, which was measured directly at the output of the active device and thus represented the switch voltage, is shown in Fig. 11. It was used to determine the class of operation of the circuit. This waveform shows a square shape for the switch voltage, which is consistent with class-F operation. The two peaks in the waveform were due to the fundamental frequency and the third harmonic. The second harmonic did not appear in the switch waveform, as it was presented with a short circuit at the output. However, in Fig. 11, it is evident that there was a significant second harmonic contribution at point **C**. This was due to the standing wave between the transistor output and the first stub, which provided the second harmonic short. Higher harmonics were not observed because the transistor did not have gain at these frequencies.
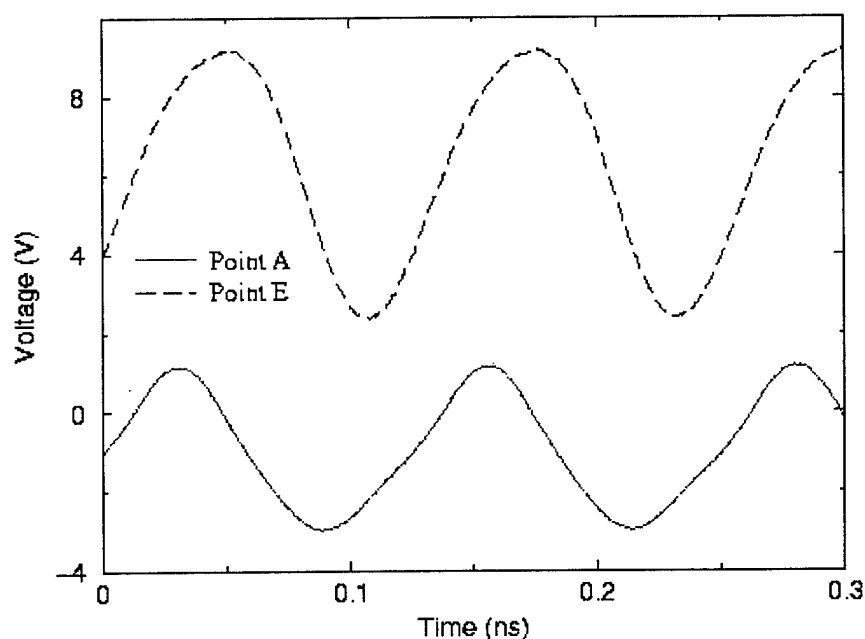

Figure 10. Photoconductive probe measurements at points A and E in the class-F amplifier circuit. This confirms that the circuit has the correct sinusoidal input and output waveforms.

Also as shown in Fig. 11, the second harmonic was not strong in the waveform at point **D**. The distortion in the waveform indicates that there was some harmonic leakage beyond the first stub. This shows that there were some improvements that could be made in the circuit to improve the purity of the output and perhaps increase efficiency. However, these photoconductive probe measurements verified essentially the existence of the proper waveforms inside the power amplifier and therefore substantiated the class-F design.

For the nonlinear microwave frequency doublers, we made internal circuit measurements at four locations: **A**, at the circuit input; **B**, immediately at the input to the active device; **C**, immediately at the output of the active device; and **D**, at the final circuit output. The waveforms

14

from within the 2.5-GHz-to-5-GHz doubler are shown in Fig. 12. At both points **A** and **B**, there was significant harmonic content, especially third harmonic. This indicates that third harmonic power was being reflected back to the input. Based on these measurements, an improved design would include a third harmonic trap at the input. At point **D**, a fairly pure sine wave at the second harmonic was seen, as desired. At the drain, point **C**, some wave shaping was seen, and some energy from the fourth, sixth, and even eighth harmonics was found in the waveform, although this is probably not sufficient to consider this class-E operation. Based on the data from the photoconductive probe measurements, it was thus also determined that more harmonic tuning would be required at the output to improve circuit operation.
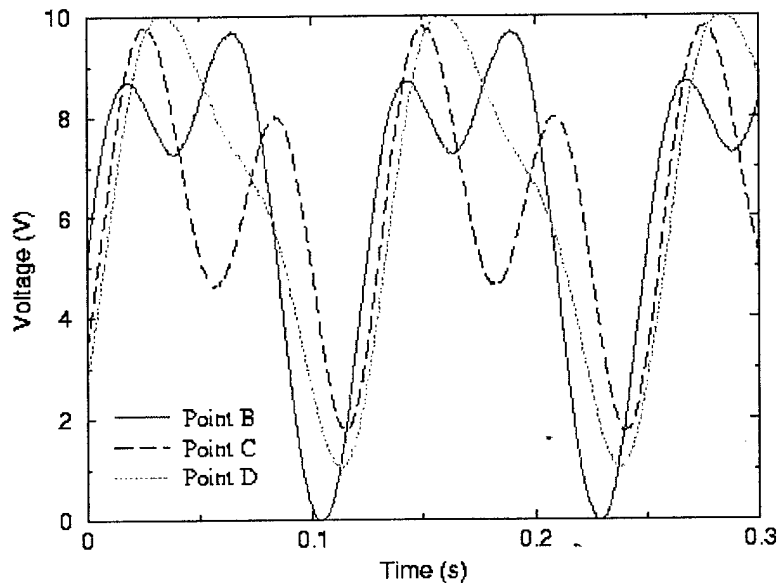

*Figure 11. Photoconductive probe measurements at points **B**, **C**, and **D** within the class-F amplifier circuit.*

Besides directly measuring the periodic waveforms with high temporal resolution (as required for high-frequency circuits), the PC probe also has high impedance (so the circuit is not disturbed), can be easily maneuvered along the microstrip to measure in many locations, and measures the absolute value of the signals captured. The realization of these nonlinear microwave measurements, which were accomplished in collaboration with Prof. Zoya Popovic at the Univ. of Colorado, has also attracted the attention of AFRL/SNDD at Wright -Patterson AFB, where it is believed that measurements of nonlinear amplifier circuits would confirm either the accuracy of existing models or the need to develop improved models.

(3) *Object reconstruction and imaging using free-space-radiating, single-cycle terahertz pulses*

A third novel ultrafast-photoconductivity application of nonstoichiometric GaAs was also explored in the latter stages of this AASERT program, utilizing LT-GaAs-based antennas as pulsed-terahertz-beam emitters and receivers in a new imaging application. Specifically, we have

shown that it is possible to exploit the broadband nature of terahertz pulses, through observation of their off-axis scattering and the subsequent manipulation of the scattered time-domain waveforms, to allow the reconstruction of the image of the scattering object. The LT-GaAs photoconductors are important not only because they can be used to generate and sample ultrashort electromagnetic pulses, but also because they are efficient (*i.e.,* they require only small amounts of laser-pulse energy for activation to a temporary low-resistivity state), and they are useful in fabricating a terahertz beam system with a high signal-to-noise ratio.
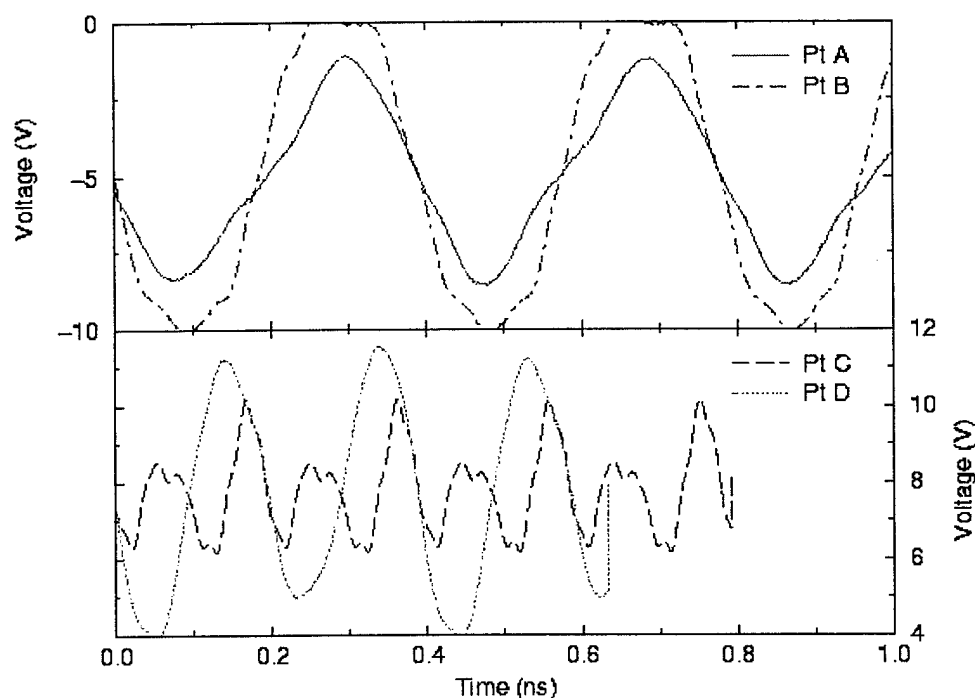

Figure 12. Waveforms measured with the photoconductive probe from within the 5-GHz microwave doubler.

Our approach is based on the time-reversal symmetry of Maxwell's equations and the Huygens-Fresnel diffraction theory. The diffraction of broadband electromagnetic pulses can be treated with the time domain Huygens-Fresnel diffraction formula, in which a superposition integral calculates a diffracted field from any given input field. Because of the time-reversal symmetry of Maxwell's equations, the diffracted field at a given position can be mathematically time-reversed and then used as an input field in the integral to reconstruct the field at the object's position. That is, it is possible to determine the (spatial) transmission function at the object by taking a THz waveform measured at several off-axis positions and applying a back-propagation algorithm to these fields. Because the time-domain THz measurement yields directly the electric field amplitude, and not just the intensity, these scattered waveforms contain all of the phase (time delay) information that is needed to obtain the spatial distribution of the electric field across the object. Intuitively, each temporal feature of the scattered waveform corresponds to the arrival of an impulse from a different region of the object. The back-propagation algorithm simply numerically differentiates the measured diffracted transient, and uses this as an input to

the time-reversed Kirchoff diffraction integral. In our experiments, the scattered fields are measured at different angles on a sphere (referred to as the "intermediate screen") centered on the object.

In our first experiments, we demonstrated the concept of time-reversal imaging using a one-dimensional object. A collimated, single-cycle THz pulse with a beam diameter of approximately 3.0-cm was incident on a 14-slit "grating" formed by Al foil strips on a low-density polyethylene (LDPE) substrate, with a periodicity, albeit irregular, of approximately 1 mm. The grating diffracted the pulse in a plane perpendicular to the grating axis, as illustrated schematically in Fig. 13. We measured the diffracted THz fields at 39 zenith positions (-32° ≤ θ ≤32°) at a radial distance of 25 cm centered on the object. This type of measurement required that the time-zero reference for all off-axis positions be maintained. This was accomplished using a THz measurement system in which femtosecond optical pulses were delivered to the emitter and detector photoconductive antennas via single-mode optical fiber. With the exception of the fiber coupling of the antennas, the system would be considered a typical time-domain THz spectrometer. This photoconductive THz system had a peak frequency of 0.425-THz (corresponding to λ_{peak}= 706 μm) with a FWHM of 421 GHz and useable frequency components up to 1.5 THz.
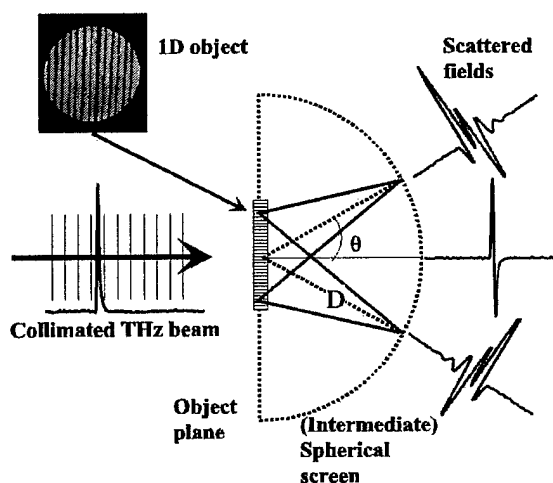

Figure 13: 1D Experimental setup. A collimated input field diffracts in all directions from an object/aperture. (The input field shown represents a field measured in the near-field of the THz emitter). The scattered transients are then recorded at different azimuths

In Fig. 14(a) we show the measured scattered THz fields at the intermediate screen. The field amplitudes at the non-zero zenith positions were magnified to accentuate the contrast relative to the forward-scattered field. For increasing non-zero angles one can observe the linear increase in the waveform period, corresponding to the later arrival times of the fields from slits at an increased separation from the detector. The object was reconstructed by using the time-reversed data of Fig. 14(a) as the input field in the time-reversed form of the Huygens-Fresnel integral for far-field diffraction from a non-planar aperture and then plotting the electric field vs. lateral position at the object. The result is shown in Fig. 14(b); the grating periodicity is clearly

17

resolved, although the edge resolution is limited by the system bandwidth. From the edge response we find the spatial resolution of the system to be approximately 500 μm.
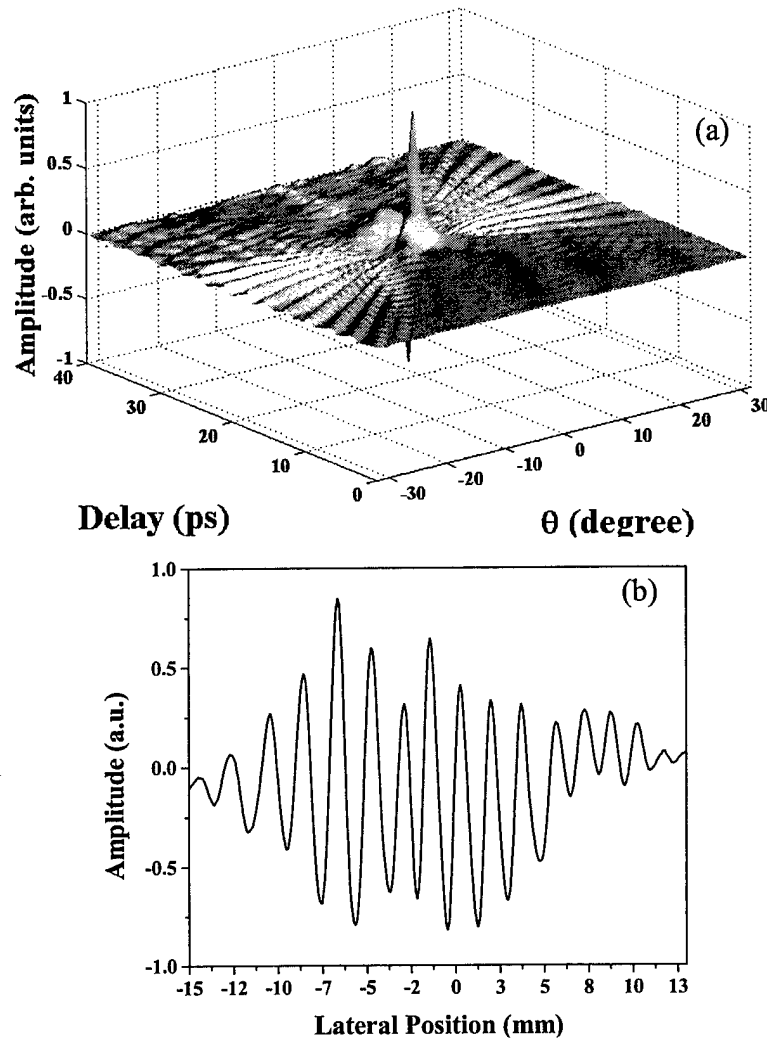

Figure 14: 1-D Experimental results: (a) the diffracted fields at the intermediate screen. These waveforms measured between ±32° were used as input (virtual) sources in the time-reversed form of the Huygens-Fresnel integral for far-field diffraction from a non-planar aperture to reproduce the transmission function of the object; the result is shown in (b).

We next demonstrated the principle of time-reversal imaging with a two-dimensional object. Ideally, in the 2-D case the scattered fields should be measured at points on a spherical grid extending over the intermediate screen in both zenith (θ) and azimuthal (ϕ) directions. Experimentally, however, it is very difficult to move the detector on a sphere centered on the object. This difficulty was circumvented by instead fixing the detector at a single angle $\theta=\theta_d \neq 0$ and rotating the object about an axis normal to its plane from 0 to 2π. Rotation in ϕ of the object is entirely equivalent to rotation of the detector on the sphere in a circle $\theta=\theta_d$, $0 \leq \phi \leq 2\pi$. Intuitively, it is clear that it is sufficient to acquire data for only one zenith angle θ, since as the object is rotated through $0 \leq \phi \leq 2\pi$, all spatial frequencies corresponding to $-\theta_d \leq \theta \leq \theta_d$ are accessed

18

for both the x and y directions in the object plane. It was then also relatively easy to perform the measurements without a fiber pig-tail to the LT-GaAs photoconductive elements. Thus, for the 2-D experiments, a conventional photoconductive free-space THz system was used; this system had a peak frequency of 156 GHz (corresponding to λ_{peak}= 1.92 mm) with a FWHM of 351 GHz and useable frequency components up to 1.0 THz. For the results shown here, the diffracted fields were measured at one zenith position (θ_d=12°) and 72 azimuthal positions (ϕ) between 0 and 2π.

In order to test the principle of 2-D time-reversal imaging using the above scheme, we first carried out a simulation, numerically propagating a single-cycle THz plane wave that approximated the spatio-temporal profile of the actual beam onto an aperture defined as a log-spiral antenna. The diffracted field was calculated for the object oriented at ϕ=0°, 5°, 10°...360° at θ_d=12°. The time-reversal image was then calculated using the time-reversed form of the Huygens-Fresnel integral and is shown in Fig. 15(b); the object is clearly imaged and corroborates the principle of ϕ-scanning for reconstruction of the object.

An experimental demonstration of the principle using these same parameters was implemented for the same object (a gold spiral antenna structure fabricated on fused silica) pictured in Fig. 15(a). The back-propagation result is shown in Fig. 15(c), where the opaque and clear portions of the aperture are clearly resolved. In fact the system was able to resolve features smaller than the peak wavelength λ_p=1.92 mm. The experimental results show excellent agreement with the ideal expected results from the computations. Note that an additional ringing response on the time-domain THz waveforms due to water absorption from the ambient air in the beam propagation path appeared clearly in the measured waveforms at the intermediate screen. This response contributes artifacts to the reconstructed image and leads to any discrepancies between the images in Figs. 15(b) and (c), although it should be possible to minimize these artifacts by applying a temporal apodization function to the experimental waveforms.

Terahertz off-axis-diffraction images were also demonstrated on dielectric objects, as well as on objects in a reflection-mode geometry.
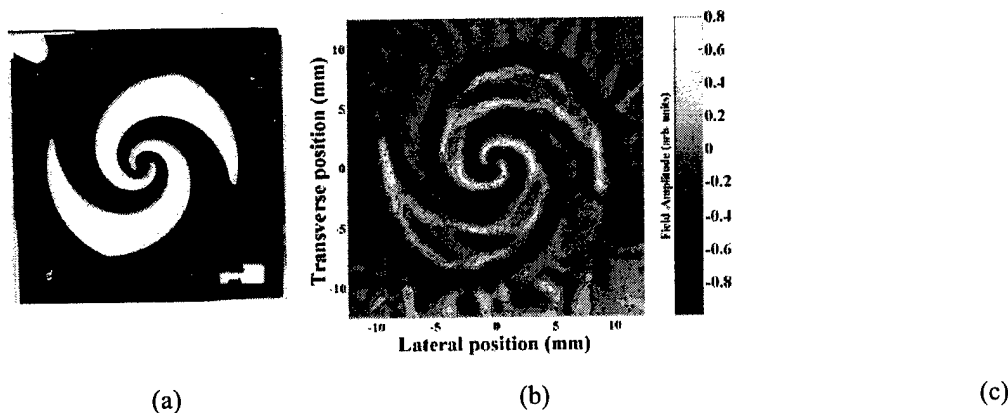

| (a) | (b) | (c) |

Fig. 15: (a) The object (aperture) from which the incident terahertz pulse was scattered in the 2-D experiment. (b) Time-reversal imaging simulation. Here, the scattered field distribution of the electric field incident on the object in (a) was calculated. The field was then time-reversed and back propagated using the same conditions as in the experiment. (c) The image obtained from the experimental data after performing the back-propagation algorithm described in the text.

19